

Light-cone-like spreading of correlations in a quantum many-body system

Marc Cheneau,^{1,*} Peter Barmettler,² Dario Poletti,² Manuel Endres,¹ Peter Schauß,¹ Takeshi Fukuhara,¹ Christian Gross,¹ Immanuel Bloch,^{1,3} Corinna Kollath,^{2,4} and Stefan Kuhr^{1,5}

¹*Max-Planck-Institut für Quantenoptik, 85748 Garching, Germany*

²*Département de physique théorique, Université de Genève, 1211 Genève, Switzerland*

³*Ludwig-Maximilians-Universität, 80799 München, Germany*

⁴*Centre de physique théorique, École Polytechnique, CNRS, 91128 Palaiseau, France*

⁵*University of Strathclyde, SUPA, Glasgow G4 0NG, United Kingdom*

How fast can correlations spread in a quantum many-body system? Based on the seminal work by Lieb and Robinson [1], it has recently been shown that several interacting many-body systems exhibit an effective light cone that bounds the propagation speed of correlations [2–5]. The existence of such a “speed of light” has profound implications for condensed matter physics and quantum information, but has never been observed experimentally. Here we report on the time-resolved detection of propagating correlations in an interacting quantum many-body system. By quenching a one-dimensional quantum gas in an optical lattice, we reveal how quasiparticle pairs transport correlations with a finite velocity across the system, resulting in an effective light cone for the quantum dynamics. Our results open important perspectives for understanding relaxation of closed quantum systems far from equilibrium [6] as well as for engineering efficient quantum channels necessary for fast quantum computations [7].

In contrast to relativistic quantum field theory, no “speed limit” exists in non-relativistic quantum mechanics, allowing in principle for the propagation of information over arbitrary distances in arbitrary short times [2]. However, one could naively expect that in real physical systems short-range interactions allow information to propagate only with a finite velocity. The existence of a maximal velocity, also called Lieb–Robinson bound, has indeed been shown theoretically in some systems, e.g. interacting spins on a lattice [2–5], but to which extent this result can be generalised remains an open question [8–11]. Lieb–Robinson bounds have already found a number of fundamental applications [12, 13]. For example, they allow for a rigorous proof of a long-standing conjecture that linked the presence of a spectral gap in a lattice system to the exponential decay of correlations in the ground state [14, 15]. They also provide fundamental scaling laws for the entanglement entropy, which is an indicator of the computational cost for simulating strongly interacting systems [16].

In the context of quantum many-body systems, the existence of a Lieb–Robinson bound can be probed by recording the dynamics following a sudden parameter change (quench) in the Hamiltonian. In that case, a simple picture has been suggested: quantum-entangled quasiparticles emerge from the initially highly excited state and propagate ballistically [3], carrying correlations across the system. Ultracold atomic gases offer an ideal testbed to explore such quantum dynamics due to their almost perfect decoupling from the environment and their fast tunability [17]. In addition, the recently demonstrated technique of single-site imaging in an optical lattice [18, 19] offers the resolution and sensitivity necessary to reveal the dynamical evolution of a many-body system at the single-particle level.

Our system consists of ultracold bosonic atoms in an optical lattice and is well described by the Bose–Hubbard model [20, 21]. This model is parameterised by two energy scales: the on-site interaction, U , and the tunnel coupling between adjacent sites, J . Driven by the competition of these two parameters, a quantum phase transition between a superfluid and a Mott-insulating phase occurs in homogeneous systems with integer filling \bar{n} . In the one-dimensional (1D) geometry considered here, the critical point of this transition is located at $(U/J)_c \simeq 3.4$ [22]. We observed the time evolution of spatial correlations after a fast decrease of the effective interaction strength U/J from an initial value deep in the Mott-insulating regime, with filling $\bar{n} = 1$, to a final value closer to the critical point (Fig. 1a). After such a quench, the initial many-body state $|\Psi_0\rangle$ is highly excited and acts as a source of quasiparticles. In order to elucidate the nature and the dynamics of these quasiparticles, we have developed an analytical model in which the occupancy of each lattice site is restricted to $n = 0, 1$ or 2 (see Appendix). For large interaction strengths, the quasiparticles consist of either an excess particle (doublon) or a hole (holon) on top of the unity-filling background. Fermionizing these quasiparticles with a Jordan–Wigner transformation allows us to partially eliminate the non-physical states in which a lattice site would be occupied by two quasiparticles. To first order in J/U , we then find that the many-body state at time t after the quench reads:

$$|\Psi(t)\rangle \simeq |\Psi_0\rangle + i\sqrt{8}\frac{J}{U}\sum_k \sin(ka_{\text{lat}}) \left[1 - e^{-i[\epsilon_d(k) + \epsilon_h(-k)]t/\hbar}\right] \hat{d}_k^\dagger \hat{h}_{-k}^\dagger |\Psi_0\rangle, \quad (1)$$

with a_{lat} the lattice period. Here \hat{d}_k^\dagger and \hat{h}_k^\dagger are the

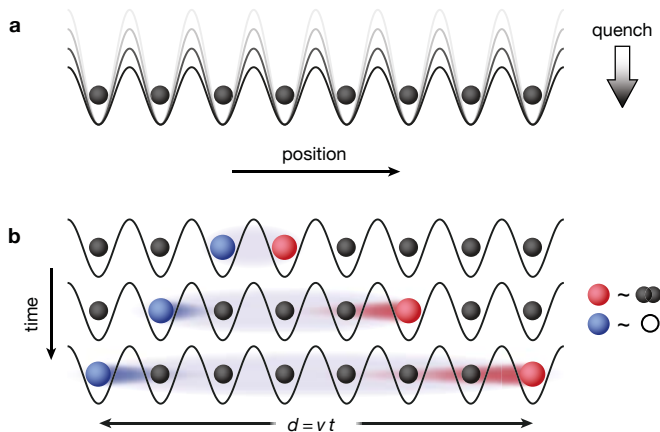


FIG. 1. **Spreading of correlations in a quenched atomic Mott insulator.** **a**, A 1D ultracold gas of bosonic atoms (black balls) in an optical lattice is initially prepared deep in the Mott-insulating phase with unity filling. The lattice depth is then abruptly lowered, bringing the system out of equilibrium. **b**, Following the quench, entangled quasiparticle pairs emerge at all sites. Each of these pairs consists of a doublon (red ball) and a holon (blue ball) on top of the unity-filling background, which propagate ballistically in opposite directions. It follows that a correlation in the parity of the site occupancy builds up at time t between any pair of sites separated by a distance $d = vt$, where v is the relative velocity of the doublons and holons.

creation operators for a doublon and a holon with momentum k , respectively, and k belongs to the first Brillouin zone. Quasiparticles thus emerge at any site in the form of entangled pairs, consisting of a doublon and a holon with opposite momenta. Some of these pairs are bound on nearest-neighbour sites while the others form wave packets, due to their peaked momentum distribution. The wave packets propagate in opposite directions with a relative group velocity v determined by the dispersion relation $\epsilon_d(k) + \epsilon_h(-k)$ of doublons and holons (Fig. 1b). The propagation of quasiparticle pairs is reflected in the two-point parity correlation functions [23]:

$$C_d(t) = \langle \hat{s}_j(t) \hat{s}_{j+d}(t) \rangle - \langle \hat{s}_j(t) \rangle \langle \hat{s}_{j+d}(t) \rangle, \quad (2)$$

where j labels the lattice sites. The operator $\hat{s}_j(t) = e^{i\pi[\hat{n}_j(t) - \bar{n}]}$ measures the parity of the occupation number $\hat{n}_j(t)$. It yields +1 in the absence of quasiparticles (odd occupancy) and -1 if a quasiparticle is present (even occupancy). Because the initial state is close to a Fock state with one atom per lattice site, we expect $C_d(t=0) \simeq 0$. After the quench, the propagation of quasiparticle pairs with the relative velocity v results in a positive correlation between any pair of sites separated by a distance $d = vt$.

The experimental sequence started with the preparation of a two-dimensional (2D) degenerate gas of ^{87}Rb confined in a single antinode of a vertical optical lattice [19, 23] (z -axis, $a_{\text{lat}} = 532 \text{ nm}$). The system was then

divided into about 10 decoupled 1D chains by adding a second optical lattice along the y -axis and by setting both lattice depths to $20.0(5) E_r$, where $E_r = (2\pi\hbar)^2 / (8ma_{\text{lat}}^2)$ is the recoil energy of the lattice and m the atomic mass of ^{87}Rb . The effective interaction strength along the chains was tuned via a third optical lattice along the x -axis. The number of atoms per chain ranged between 10 and 18, resulting in a lattice filling $\bar{n} = 1$ in the Mott-insulating domain. The initial state was prepared by adiabatically increasing the x -lattice depth until the interaction strength reached a value of $(U/J)_0 = 40(2)$. At this point, we measured the temperature to be $T \simeq 0.1 U/k_B$ (k_B is the Boltzmann constant) following the method described in Ref. [19]. We then brought the system out of equilibrium by lowering the lattice depth typically within 100 μs , which is fast compared to the inverse tunnel coupling \hbar/J , but still adiabatic with respect to transitions to higher Bloch bands. The final lattice depths were in the Mott-insulating regime, close to the critical point. After a variable evolution time, we “froze” the density distribution of the many-body state by rapidly raising the lattice depth in all directions to $\sim 80 E_r$. Finally, the atoms were detected by fluorescence imaging using a microscope objective with a resolution on the order of the lattice spacing and a reconstruction algorithm extracted the occupation number at each lattice site [19]. Because inelastic light-assisted collisions during the imaging lead to a rapid loss of atom pairs, we directly detected the parity of the occupation number.

Our experimental results for the time evolution of the two-point parity correlations after a quench to $U/J = 9.0(3)$ show a clear positive signal propagating with increasing time to larger distances d (Fig. 2). In addition, the propagation velocity of the correlation signal is constant over the range $2 \leq d \leq 6$ (inset of Fig. 2). We found similar dynamics also for quenches to $U/J = 5.0(2)$ and $7.0(3)$ (Fig. 4). We note that the observed signal cannot be attributed to a simple density wave because such an excitation would result in $\langle \hat{s}_j \hat{s}_{j+d} \rangle = \langle \hat{s}_j \rangle \langle \hat{s}_{j+d} \rangle$. We compared the experimental results to numerical simulations of an infinite, homogeneous system at $T = 0$ using the adaptive time-dependent density matrix renormalization group [24, 25] (t -DMRG). In the simulation, the initial and final interaction strengths were fixed at the experimentally determined values and the quench was considered instantaneous, at $t = 0$. We found remarkable agreement between the experiment and theory over all explored distances and times, despite the finite temperature and the harmonic confinement with frequency $\nu = 68(1) \text{ Hz}$ that characterise the experimental system. The observed dynamics is also qualitatively reproduced by our analytical model for $U/J = 9.0$. For lower values of U/J , however, the model breaks down due to the increasing number of quasiparticles.

We extracted the propagation velocity v from the time of the correlation peak as a function of the distance

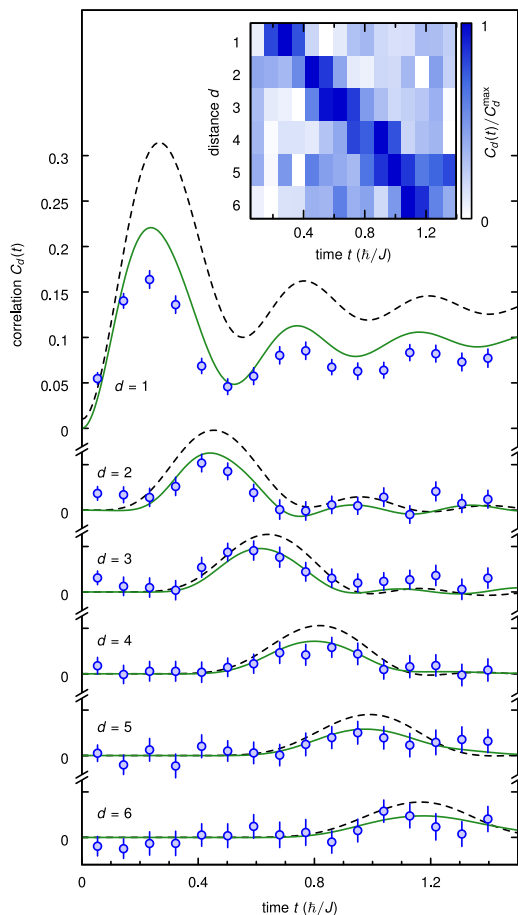


FIG. 2. Time evolution of the two-point parity correlations. After the quench, a positive correlation signal propagates with increasing time to larger distances. The experimental values for a quench from $U/J = 40$ to $U/J = 9.0$ (circles) are in good agreement with the corresponding numerical simulation for an infinite, homogeneous system at zero temperature (continuous line). Our analytical model (dashed line) also qualitatively reproduces the observed dynamics. Inset: Experimental data displayed as a colormap, revealing the propagation of the correlation signal with a well defined velocity. The experimental values result from the average over the central N sites of more than 1000 chains, where N equals 80% of the length of each chain. Error bars represent the standard deviation.

d (Fig. 3a). A linear fit restricted to $2 \leq d \leq 6$ yields $v \times \hbar/(Ja_{\text{lat}}) = 5.0(2)$, $5.6(5)$ and $5.0(2)$ for $U/J = 5.0(2)$, $7.0(3)$ and $9.0(3)$, respectively. The points for $d = 1$ were excluded from the fit, as they result from the interference between propagating and bound quasi-particle pairs (see Eq. 1). A comparison of the experimental velocities with the ones obtained from numerical simulations (Fig. 3b) shows agreement within the error bars. The measured velocities can also be compared with two limiting cases: On the one hand, they are significantly larger than the spreading velocity of non-interacting particles, $v = 4Ja_{\text{lat}}/\hbar$, and twice the

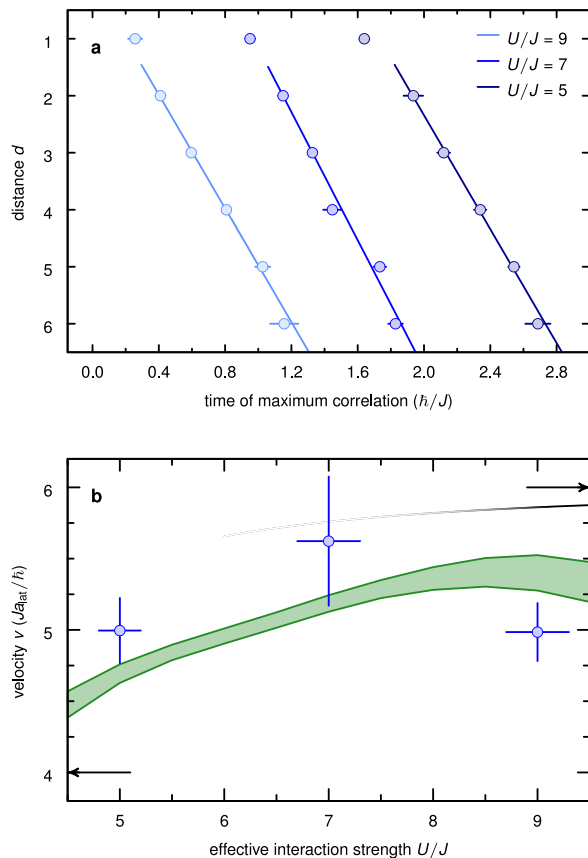


FIG. 3. Propagation velocity. **a**, Determination of the propagation velocity for the quenches to $U/J = 5.0$ (triangles), 7.0 (squares) and 9.0 (circles). The time of the maximum of the correlation signal is obtained from fits to the traces $C_d(t)$. Error bars represent the 68% confidence interval of these fits. We then extract the propagation velocities from weighed linear fits restricted to $2 \leq d \leq 6$ (lines). The data for $U/J = 5.0$ and 7.0 have been offset horizontally for clarity. **b**, Comparison of the experimental velocities (circles) to the ones obtained from numerical simulations for an infinite, homogeneous system at zero temperature (shaded area). The shaded area and the vertical error bars denote the 68% confidence interval of the fit. The horizontal error bars represent the uncertainty due to the calibration of the lattice depth. The black line corresponds to the bound v_{max} predicted by our effective model (the fading indicates the break down of this model). The arrows mark the maximum velocity expected in the non-interacting case (left) and the asymptotic value derived from our model when $U/J \rightarrow \infty$ (right).

velocity of sound in the superfluid phase [26]; on the other hand, they remain below the maximum velocity $v_{\text{max}} \approx (6Ja_{\text{lat}}/\hbar) [1 - 16J^2/(9U^2)]$ predicted by our analytical model, that can be interpreted as a Lieb-Robinson bound (Fig. 3b). In the limit $U/J \rightarrow \infty$, this bound corresponds to doublons and holons propagating with the respective group velocities $4Ja_{\text{lat}}/\hbar$ and $2Ja_{\text{lat}}/\hbar$. The higher velocity of doublons simply reflects their Bose-enhanced tunnel coupling.

In conclusion, we have presented the first experimen-

tal observation of an effective light cone for the spreading of correlations in an interacting quantum many-body system. Although the observed dynamics can be understood within a fermionic quasiparticle picture valid deep in the Mott insulating regime, we note that our experimental data cover a region close to the critical point, for which only ab-initio numerical simulations are available so far [8]. Our work opens interesting perspectives, such as revealing the entanglement carried by the quasiparticle pairs or investigating the quantum dynamics in higher dimensions, where little is known about Lieb–Robinson bounds and the scaling of entanglement. For example, the experiment can be extended to study correlation propagation in two dimensions, where existing numerical and analytical approaches suffer from severe limitations. Furthermore, the production rate of excitations and the domain formation when tuning the effective interaction strength slowly across the critical point can be investigated, thereby exploring a quantum analog to the Kibble–Zurek mechanism [6, 27, 28].

ACKNOWLEDGEMENTS

We thank C. Weitenberg and J. F. Sherson for their contribution to the design and construction of the apparatus. We also thank D. Baeriswyl, T. Giamarchi, V. Gritsev and S. Huber for discussions. C.K. acknowledges previous collaboration on a related subject with A. Läuchli. We acknowledge funding by MPG, DFG, EU (NAMEQUAM, AQUATE, Marie Curie Fellowship to M.C.), JSPS (Postdoctoral Fellowship for Research Abroad to T.F.), “Triangle de la physique”, ANR (FAMOUS) and SNSF (under division II). Financial support for the computer cluster on which the calculations were performed has been provided by the “Fondation Ernst et Lucie Schmidheiny”.

* Electronic address: marc.cheneau@mpq.mpg.de

- [1] E. H. Lieb and D. W. Robinson, *Commun. Math. Phys.*, **28**, 251 (1972).
- [2] S. Bravyi, M. B. Hastings, and F. Verstraete, *Phys. Rev. Lett.*, **97**, 050401 (2006).
- [3] P. Calabrese and J. Cardy, *Phys. Rev. Lett.*, **96**, 136801 (2006).
- [4] J. Eisert and T. J. Osborne, *Phys. Rev. Lett.*, **97**, 150404 (2006).
- [5] B. Nachtergaele, Y. Ogata, and R. Sims, *J. Stat. Phys.*, **124**, 1 (2006).
- [6] A. Polkovnikov, K. Sengupta, A. Silva, and M. Vengalattore, *Rev. Mod. Phys.*, **83**, 863 (2011).
- [7] S. Bose, *Contemp. Phys.*, **48**, 13 (2007).
- [8] A. M. Läuchli and C. Kollath, *J. Stat. Mech.*, P05018 (2008).
- [9] B. Nachtergaele, H. Raz, B. Schlein, and R. Sims, *Commun. Math. Phys.*, **286**, 1073 (2009).
- [10] M. Cramer, A. Serafini, and J. Eisert, in *Quantum Information and Many Body Quantum Systems*, CRM, Vol. 8, Publications of the Scuola Normale Superiore (Edizioni della Normale, Pisa, 2008) pp. 51–72.
- [11] J. Eisert and D. Gross, *Phys. Rev. Lett.*, **102**, 240501 (2009).
- [12] M. B. Hastings, *Phys. Rev. B*, **69**, 104431 (2004).
- [13] B. Nachtergaele and R. Sims, (2011), arXiv:1102.0835.
- [14] B. Nachtergaele and R. Sims, *Commun. Math. Phys.*, **265**, 119 (2006).
- [15] M. B. Hastings and T. Koma, *Commun. Math. Phys.*, **265**, 781 (2006).
- [16] J. Eisert, M. Cramer, and M. B. Plenio, *Rev. Mod. Phys.*, **82**, 277 (2010).
- [17] I. Bloch, J. Dalibard, and W. Zwerger, *Rev. Mod. Phys.*, **80**, 885 (2008).
- [18] W. S. Bakr, J. I. Gillen, A. Peng, S. Fölling, and M. Greiner, *Nature*, **462**, 74 (2009).
- [19] J. F. Sherson, C. Weitenberg, M. Endres, M. Cheneau, I. Bloch, and S. Kuhr, *Nature*, **467**, 68 (2010).
- [20] M. P. A. Fisher, P. B. Weichman, G. Grinstein, and D. S. Fisher, *Phys. Rev. B*, **40**, 546 (1989).
- [21] D. Jaksch, C. Bruder, J. I. Cirac, C. W. Gardiner, and P. Zoller, *Phys. Rev. Lett.*, **81**, 3108 (1998).
- [22] T. D. Kühner, S. R. White, and H. Monien, *Phys. Rev. B*, **61**, 12474 (2000).
- [23] M. Endres, M. Cheneau, T. Fukuhara, C. Weitenberg, P. Schauß, C. Gross, L. Mazza, M. C. Bañuls, L. Pollet, I. Bloch, and S. Kuhr, *Science*, **334**, 200 (2011).
- [24] A. J. Daley, C. Kollath, U. Schollwöck, and G. Vidal, *J. Stat. Mech.*, **2004**, P04005 (2004).
- [25] S. R. White and A. E. Feiguin, *Phys. Rev. Lett.*, **93**, 076401 (2004).
- [26] C. Kollath, U. Schollwöck, J. von Delft, and W. Zwerger, *Phys. Rev. A*, **71**, 053606 (2005).
- [27] T. W. B. Kibble, *J. Phys. A-Math. Gen.*, **9**, 1387 (1976).
- [28] W. H. Zurek, *Nature*, **317**, 505 (1985).
- [29] C. D. Batista and G. Ortiz, *Phys. Rev. Lett.*, **86**, 1082 (2001).
- [30] S. D. Huber, E. Altman, H. P. Büchler, and G. Blatter, *Phys. Rev. B*, **75**, 085106 (2007).
- [31] E. Altman and A. Auerbach, *Phys. Rev. Lett.*, **89**, 250404 (2002).
- [32] U. Schollwöck, *Ann. Phys. (N.Y.)*, **326**, 96 (2011).
- [33] G. Vidal, *Phys. Rev. Lett.*, **98**, 070201 (2007).
- [34] I. P. McCulloch, (2008), arXiv:0804.2509.
- [35] S. R. White, *Phys. Rev. Lett.*, **69**, 2863 (1992).

APPENDIX

Quenches to $U/J = 5.0$ and 7.0

We also recorded the time evolution of the two-point parity correlations (2) after quenches to $U/J = 5.0(2)$ and $7.0(3)$, and compared the experimental results to DMRG simulations of an infinite, homogeneous system at zero temperature (Fig. 4). The experimental sequence was identical to the one we used for the quench to $U/J = 9.0(3)$, apart from the different end point of the quench. The data presented here are those used in Fig. 3.

Quasiparticle model

In the Bose–Hubbard model, bosonic atoms in an optical lattice are confined to a single Bloch band and obey the Hamiltonian

$$\hat{H} = \sum_j \left\{ -J (\hat{a}_j^\dagger \hat{a}_{j+1} + \text{h.c.}) + \frac{U}{2} \hat{n}_j (\hat{n}_j - 1) \right\}, \quad (3)$$

where \hat{a}_j and \hat{a}_j^\dagger represent the annihilation and creation operator of an atom at site j and $\hat{n}_j = \hat{a}_j^\dagger \hat{a}_j$ counts the

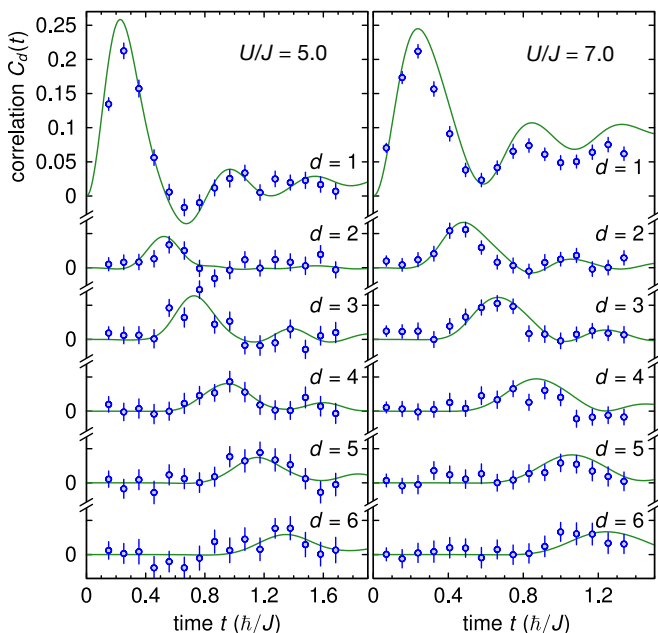


FIG. 4. **Time evolution of the two-point parity correlations.** Left panel: quench to $U/J = 5.0(2)$. Right panel: quench to $U/J = 7.0(3)$. The circles indicate the correlations measured experimentally and the line is derived from the numerical simulations for an infinite, homogeneous system at zero temperature. The experimental and numerical values were obtained in the same way as described in the legend of Fig. 2 and in the Methods Summary section.

number of atoms at that site. The model is entirely parametrised by the effective interaction strength U/J .

In order to analytically treat the time evolution of correlations after a sudden decrease of U/J , we developed a novel approach based on fermionized quasiparticles. The initial state being close to a Fock state with one atom per lattice site, an effective description of the evolution at sufficiently large final interaction strengths can be obtained within a local basis formed by empty states, $|\circ\rangle_j$, singly occupied states, $|\bullet^\circ\rangle_j$, and doubly occupied states, $|\bullet^\bullet\rangle_j$. Using generalised Jordan–Wigner transformations [29], we then introduced fermionic creation operators for the excess particles, $\hat{d}_j^\dagger |\circ\rangle_j \rightarrow |\bullet^\bullet\rangle_j$, and the holes, $\hat{h}_j^\dagger |\bullet^\circ\rangle_j \rightarrow |\circ\rangle_j$, as well as the corresponding annihilation operators. Within the truncated Hilbert space, the original Hamiltonian (3) can be exactly written in terms of these operators:

$$\hat{H} = \sum_j \hat{\mathcal{P}} \left\{ -2J \hat{d}_j^\dagger \hat{d}_{j+1} - J \hat{h}_{j+1}^\dagger \hat{h}_j - J\sqrt{2} (\hat{d}_j^\dagger \hat{h}_{j+1}^\dagger - \hat{h}_j \hat{d}_{j+1}) + \text{h.c.} + \frac{U}{2} (\hat{n}_{d,j} + \hat{n}_{h,j}) \right\} \hat{\mathcal{P}}, \quad (4)$$

with $\hat{n}_{d,j} = \hat{d}_j^\dagger \hat{d}_j$ and $\hat{n}_{h,j} = \hat{h}_j^\dagger \hat{h}_j$. The complexity of the model is hidden in the projector $\hat{\mathcal{P}} = \prod_j (\hat{I} - \hat{n}_{d,j} \hat{n}_{h,j})$ that eliminates the unphysical situation of having an excess particle and a hole at the same site (\hat{I} is the identity operator). As multiple occupancies of equal species are naturally avoided due to their statistics, one still obtains a good description of the system when setting $\hat{\mathcal{P}} \rightarrow \hat{I}$, provided the density of excitations $\langle \hat{n}_{d,j}(t) + \hat{n}_{h,j}(t) \rangle$ remains low. This is in contrast to the usual bosonic representations [30, 31].

The Hamiltonian (4) with $\hat{\mathcal{P}} \rightarrow \hat{I}$ is quadratic and can be diagonalised by a Bogolyubov transformation. The eigenmodes are *doublons* and *holons* with well defined momentum k :

$$\hat{\gamma}_{d,k}^\dagger = u(k) \hat{d}_k^\dagger + v(k) \hat{h}_{-k}, \quad (5)$$

$$\hat{\gamma}_{h,-k}^\dagger = u(k) \hat{h}_{-k}^\dagger - v(k) \hat{d}_k, \quad (6)$$

with

$$u(k) = \cos[\theta(k)/2], \quad v(k) = i \sin[\theta(k)/2]$$

$$\text{and } \theta(k) = \text{atan} \left[\frac{\sqrt{32}J \sin(ka_{\text{lat}})}{U - 6J \cos(ka_{\text{lat}})} \right]. \quad (7)$$

Their respective eigenenergies are given by

$$\epsilon_d(k) = -J \cos(ka_{\text{lat}}) + \frac{1}{2} \sqrt{[U - 6J \cos(ka_{\text{lat}})]^2 + 32J^2 \sin^2(ka_{\text{lat}})}, \quad (8)$$

$$\epsilon_h(k) = J \cos(ka_{\text{lat}}) + \frac{1}{2} \sqrt{[U - 6J \cos(ka_{\text{lat}})]^2 + 32J^2 \sin^2(ka_{\text{lat}})}. \quad (9)$$

Within this model, the initial state $|\psi_0\rangle$ evolves in time according to:

$$|\psi(t)\rangle = e^{-i\hat{H}t/\hbar} |\psi_0\rangle \quad (10)$$

$$= \prod_k \left\{ \bar{u}(k) - \bar{v}(k) e^{-i[\epsilon_d(k) + \epsilon_h(-k)]t/\hbar} \cdot \hat{\gamma}_{d,k}^\dagger \hat{\gamma}_{h,-k}^\dagger \right\} |\text{vac}\rangle, \quad (11)$$

with

$$\bar{u}(k) = u(k)u_0(k) - v(k)v_0(k), \quad (12)$$

$$\bar{v}(k) = v(k)u_0(k) - u(k)v_0(k). \quad (13)$$

Here the subscript ‘‘0’’ denotes quantities corresponding to the initial interaction strength, whereas no label is used for the quantities corresponding to the final interaction strength. Further, $|\text{vac}\rangle$ represents the quasiparticle vacuum at the final interaction strength ($\hat{\gamma}_{d,k}|\text{vac}\rangle = \hat{\gamma}_{h,k}|\text{vac}\rangle = 0$). Equation (10) describes wave packets of entangled quasiparticle pairs that travel in opposite directions with different velocities. One can extract a maximal velocity for the spreading of the correlations from the dispersion relation of a quasiparticle pair (black line in Fig. 3b):

$$v_{\text{max}} = \frac{1}{\hbar} \max_k \left\{ \frac{d}{dk} |\epsilon_d(k) + \epsilon_h(k)| \right\}. \quad (14)$$

Additionally, we derived from equation (10) the time evolution of the two-point parity correlations. In agreement with DMRG simulations, it displays a clear positive signal, the position of which increases with time (Fig. 2). We extracted the instantaneous propagation velocity $v(d_0)$ from a linear fit through the signal positions $d_0 \leq d \leq d_0 + 4$ (Fig. 5). The case $d_0 = 2$ corresponds to the data shown in Fig. 3. At short distances, we find velocities about 10 % smaller than v_{max} , in good agreement with the velocities measured experimentally. At large distances, the velocity converges algebraically to v_{max} . This latter behaviour can be understood from the expansion of the correlation functions to first order in J/U , which can be expressed in terms of the Airy function $\text{Ai}(x)$:

$$C_d(t) \stackrel{d \gg 1}{\simeq} \left[\frac{2^{7/3} d^{2/3} \hbar}{3Ut} \text{Ai} \left[(2/d)^{1/3} (d - 6Jt/\hbar) \right] \right]^2. \quad (15)$$

We checked the validity of our model of freely propagating fermionic quasiparticles by comparing it with DMRG simulations. The propagation velocity of the two-point parity correlations is very accurate in the strongly interacting limit (e.g. $U/J = 20$), and remains in fairly good agreement down to $U/J = 9$, where the quasiparticle density is about 0.1 per site (Fig. 5). At lower interaction strengths, we found that the Gutzwiller approximation breaks down. Nevertheless, the experiment and the simulations show that the spreading of correlations is still characterised by a well defined velocity, for which

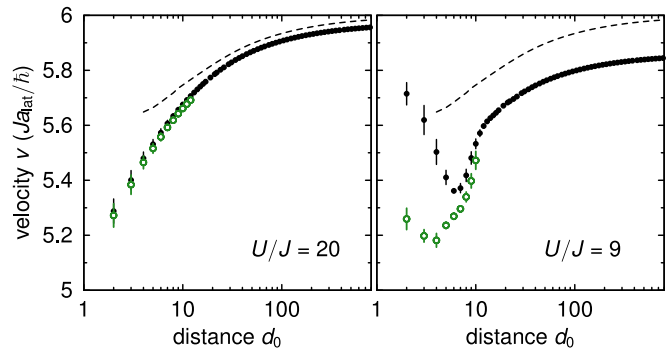


FIG. 5. **Instantaneous propagation velocity.** We compare the instantaneous velocity $v(d_0)$ predicted by our analytical model (points) with the one derived from numerical simulations (circles). The agreement is excellent at $U/J = 20$ (left panel) and qualitatively good at $U/J = 9$ (right panel). Error bars denote the 68 % confidence interval of the fit. The dashed line represents the asymptotic expression (15). Arrows point to the maximum velocity v_{max} at the given interaction strength. The signal position was obtained using the procedure described in the Methods Summary section for the numerical simulations.

v_{max} remains a relevant upper bound. We verified numerically that the truncation of the local Hilbert space to three states is reasonable down to $U/J \simeq 6$.

Calibration of the lattice depth

We calibrated the lattice depths by performing amplitude modulation spectroscopy of the transition between the zeroth and second Bloch band on a 1D degenerate gas for the x - and y -axes, and on a 2D degenerate gas for the z -axis. We estimate the calibration uncertainty to be 1–2%.

Bose–Hubbard parameters

For a given lattice depth V , we calculated the tunnel coupling and the on-site interaction of the Bose–Hubbard model (3) in the single-particle picture using their expressions as overlap integrals of the Wannier functions. In Table I, we provide the values of V , J and U for the effective interaction strengths mentioned in the main text.

Ramp of the lattice depth for the quench

The ramp of the lattice depth for the quench follows the functional form:

$$V(t) = V_0 + (V - V_0) \frac{e^{-t/\tau} - 1}{e^{-T/\tau} - 1}. \quad (16)$$

U/J	$V (E_r)$	$J/\hbar (s^{-1})$	$U/h (Hz)$
40(2)	13.5(2)	113(5)	724(4)
9.0(3)	7.70(11)	422(11)	607(3)
7.0(3)	6.85(11)	522(14)	584(3)
5.0(2)	5.75(13)	691(23)	550(4)

TABLE I. Lattice depth and Bose–Hubbard parameters for the data reported in the main text. The lattice depth in the perpendicular axes is $20.0(5) E_r$. The uncertainties on J , U and U/J follow from the calibration uncertainty on the lattice depth (see Methods Summary).

U/J	$T (\mu s)$	$\tau (\mu s)$
9.0	100	130
7.0	100	120
5.0	150	160

TABLE II. Lattice depth ramp parameters used for the quenches reported in the main text, as defined in equation (16).

Here $V_0 = 13.5 E_r$ is the initial lattice depth, T is the duration of the ramp and τ determines the rate at which the lattice depth is decreased. These parameters have to be chosen such that the ramp is fast compared to the time scale of the dynamics following the quench, which is given by \hbar/J , but adiabatic with regard to transitions to higher Bloch bands. The latter condition requires the parameter $\Gamma = (\hbar/\Delta^2)|d\Delta/dt|$ to be much smaller than 1, where Δ is the energy gap between the two Bloch bands considered. For each quench, we have chosen the ramp parameters such that T is the shortest ramp duration

compatible with $\Gamma < 0.3$ (Table II).

Numerical simulations showed that the origin $t = 0$ of the time evolution can be defined as the moment when the effective interaction strength reaches the value $U/J \simeq 17$. We used the same phenomenological criterion to locate the moment at which the dynamics stops when raising the lattice depth to $\sim 80 E_r$.

Determination of the time of the correlation peak

We extracted the time of the maximum of the correlation signal as a function of the distance, for both the experiment and the theory, by fitting an offset-free gaussian profile to the traces $C_d(t)$. For the numerical data, we filtered out frequency components above $3J/\hbar$ prior to the fit in order to isolate the envelope of the signal. For the experimental data, we fixed the width of the gaussian profile to the value obtained from the numerical data, keeping only the amplitude and time as free parameters.

Numerical simulations

The numerical simulations relied on matrix product states [32] (MPS) to represent infinite homogenous systems [33, 34]. Initial states were obtained using the DMRG algorithm [35]. For the time evolution, we used a second-order Suzuki–Trotter decomposition [24, 25]. We achieved quasi-exact results on the relevant time scale $tJ/\hbar \sim 2$ by choosing a small enough Trotter time step (~ 0.002) and retaining a few thousand states.